CHANNELS
2024, VOL. 18, NO. 1, 2396346
https://doi.org/10.1080/19336950.2024.2396346

Taylor & Francis
Taylor & Francis Group

RESEARCH ARTICLE

OPEN ACCESS Check for updates

Evaluation of four *KCNMA1* channelopathy variants on BK channel current under $Ca_V1.2$ activation

Ria L. Dinsdale and Andrea L. Meredith

Department of Physiology, University of Maryland School of Medicine, Baltimore, MD, USA

ABSTRACT

Variants in *KCNMA1*, encoding the voltage- and calcium-activated K^+ (BK) channel, are associated with human neurological disease. The effects of gain-of-function (GOF) and loss-of-function (LOF) variants have been predominantly studied on BK channel currents evoked under steady-state voltage and Ca^{2+} conditions. However, in their physiological context, BK channels exist in partnership with voltage-gated Ca^{2+} channels and respond to dynamic changes in intracellular Ca^{2+} ($Ca^{2+}{}_i$). In this study, an L-type voltage-gated Ca^{2+} channel present in the brain, $Ca_V1.2$, was co-expressed with wild type and mutant BK channels containing GOF (D434G, N999S) and LOF (H444Q, D965V) patient-associated variants in HEK-293T cells. Whole-cell BK currents were recorded under $Ca_V1.2$ activation using buffering conditions that restrict $Ca^{2+}{}_i$ to nano- or micro-domains. Both conditions permitted wild type BK current activation in response to $Ca_V1.2$ Ca^{2+} influx, but differences in behavior between wild type and mutant BK channels were reduced compared to prior studies in clamped $Ca^{2+}{}_i$. Only the N999S mutation produced an increase in BK current in both micro- and nano-domains using square voltage commands and was also detectable in BK current evoked by a neuronal action potential within a microdomain. These data corroborate the GOF effect of N999S on BK channel activity under dynamic voltage and Ca^{2+} stimuli, consistent with its pathogenicity in neurological disease. However, the patient-associated mutations D434G, H444Q, and D965V did not exhibit significant effects on BK current under $Ca_V1.2$-mediated Ca^{2+} influx, in contrast with prior steady-state protocols. These results demonstrate a differential potential for *KCNMA1* variant pathogenicity compared under diverse voltage and Ca^{2+} conditions.

ARTICLE HISTORY
Received 24 June 2024
Revised 14 August 2024
Accepted 20 August 2024

KEYWORDS
$K_{Ca}1.1$; calcium-activated potassium channel; *channelopathy*; $Ca_V1.2$; voltage-gated calcium channels; *CACNA1C*

Introduction

Channelopathy disorders are caused by gene mutations producing pathological deficits in ion channel function. In humans, *KCNMA1* gene mutations underlie a rare neurological disorder associated with dysfunction of BK channels. *KCNMA1* transcripts are widely expressed in the central nervous system, and the *KCNMA1*-linked channelopathy disorder has multiple brain manifestations, including dyskinesia, epilepsy, developmental delay, and intellectual disability [1–3]. Patient-associated *KCNMA1* variants have been designated as gain-of-function (GOF) or loss-of-function (LOF) in BK channel activity based on experiments conducted under steady-state voltage and clamped the intracellular free calcium concentration ($[Ca^{2+}]_i$) in HEK293 and CHO cells. How BK channel dysfunction in vivo produces neurological disease is still under investigation [1,4–12].

BK channels are members of the voltage-activated potassium channel family. They are activated by depolarizing transmembrane voltage and by intracellular Ca^{2+} through the direct binding of calcium to two intracellular sites within the C-terminal gating ring [13]. These properties make BK channel activation responsive to dynamic Ca^{2+} signaling in neurons at physiological membrane potentials [14], as $[Ca^{2+}]_i$ in neurons increases from resting conditions of <100 nM to as high as 700 nM upon stimulation [15]. Neuronal BK channel opening typically depends on local $[Ca^{2+}]_i$ provided by multiple types of voltage-gated Ca^{2+} channels (Ca_V) and Ca^{2+}-permeable channels [14,16]. While physical details of BK-Ca_V interactions are not fully elucidated, the evidence suggests that BK channels interact with the Ca_V α1 subunit and Ca_V auxiliary subunits [17,18] in a manner that varies with cell type and excitable signaling [14].

CONTACT Andrea L. Meredith ameredith@som.umaryland.edu
Supplemental data for this article can be accessed online at https://doi.org/10.1080/19336950.2024.2396346

Ca_V-mediated BK channel activation occurs within diffusion-restricted membrane domains: microdomains (10–100 nm) and nanodomains (<10 nm) [14,19,20]. These domains can be investigated experimentally by recording BK channel currents under ethylene glycol tetraacetic acid (EGTA) or 1,2-bis(o-aminophenoxy) ethane-N,N,N′,N′-tetraacetic acid (BAPTA) buffering conditions. EGTA is a slow Ca^{2+} chelator that restricts Ca^{2+} diffusion over longer distances. BAPTA has a similar binding affinity to EGTA, but greater on-rate, restricting Ca^{2+} diffusion over shorter distances [21]. Single-molecule localization experiments revealed that voltage-activated $Ca_V1.3$ channels closely cluster within 10–20 nM of BK channels in rat hippocampal and sympathetic neurons and in heterologous tsA-201 cells [22]. Models developed from electrophysiological data estimate that BK channels in these clusters could encounter 20 μM $Ca^{2+}{}_i$ under endogenous conditions or in the presence of EGTA buffering (microdomain conditions) and >5 μM $Ca^{2+}{}_i$ under BAPTA (nanodomain) buffering conditions [16,23](Figure 1a). BK activation via Ca_V coupling is rapid (within a millisecond), regulated by the specific BK and Ca_V subunits present, and differentially sensitive to EGTA and BAPTA under different cellular conditions [14,18,22–31]. Despite the specificity of Ca_V-mediated BK channel activation in neuronal signaling, the details of BK-Ca_V function in neurological disease is not well studied.

$Ca_V1.2$ is a widely expressed L-type voltage gated Ca^{2+} channel that influences central neuronal excitability [32] and was previously shown to partner with BK channels [24,27,28,33]. In heterologous cells, $Ca_V1.2$ channels comprised $Ca_V1.2$ α1 (*CACNA1C*), α2δ1, and β1b operate between −30 mV and +60 mV, with a peak activation at 0 mV that overlaps with BK channel voltage sensitivity [27], and mutations in BK and $Ca_V1.2$ channels have some overlapping neurological dysfunctions, including epilepsy, developmental delay, and intellectual disability [1,34]. The consequences of *KCNMA1* channelopathy variants that alter BK channel gating properties have not been investigated under BK-$Ca_V1.2$ channel coupled activation. In this study, four *KCNMA1* variants previously studied under clamped Ca^{2+} conditions

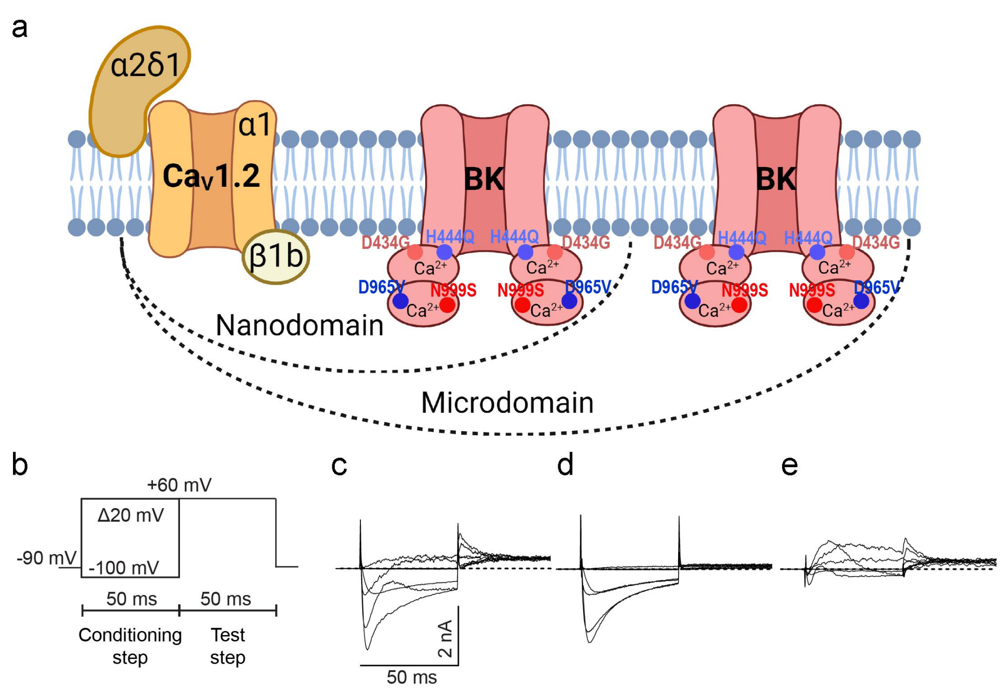

Figure 1. BK channel activation by Ca^{2+} influx through $Ca_V1.2$ channels. (a) $Ca_V1.2$ and BK channel subunits in 2 mM BAPTA and 10 mM EGTA delimited buffering domains. (b) Two-step voltage protocol used to elicit whole-cell $Ca_V1.2$ currents (conditioning step), followed by BK currents (test step). (c) Total current from HEK-293T cells co-expressing $Ca_V1.2$ and BK channels recorded in 10 mM EGTA. (d) Inward $Ca_V1.2$ current isolated by addition of 100 nM paxilline to block BK current. (e) Outward BK channel currents obtained by subtracting (d) from (c). Dotted line represents the zero current level.

(two GOF and two LOF) were investigated in BK channels activated under $Ca_V1.2$ channel Ca^{2+} influx.

In recordings made in clamped Ca^{2+}, BK channels containing the well-studied *KCNMA1* channelopathy mutations D434G and N999S (BK^{D434G} and BK^{N999S}) exhibit GOF behavior, shifting voltage-dependent activation toward more hyperpolarized potentials over a range of $[Ca^{2+}]_i$ from 0–100 μM [4,12,35–42]. Along with shifting the conductance-voltage (G-V) relationship, the D434G and N999S mutations also alter BK channel kinetics, causing faster activation and slower deactivation [4,12,36–42]. BK^{N999S} channels show a greater shift in the G-V curve and a faster channel activation compared to BK^{D434G} channels [4,37]. The LOF *KCNMA1* variants H444Q and D965V (BK^{H444Q} and BK^{D965V}) produce channels with G-V relationships shifted toward more depolarized membrane potentials by 23 mV and 40 mV, respectively, and decrease activation kinetics compared to wild type BK channels [4,12,43]. BK^{H444Q} also exhibits faster deactivation kinetics [12,43]. The effect of these four representative mutations was investigated by co-expressing BK^{WT}, BK^{N999S}, BK^{D434G}, BK^{H444Q}, or BK^{D965V} channels with $Ca_V1.2$ channels in HEK-293 cells and recording whole-cell currents under voltage-clamp. GOF and LOF activities in $Ca_V1.2$-activated BK currents were compared to previous functional studies in clamped Ca^{2+} conditions to assess the congruency.

Methods

Cell culture and transfection

Mutations were introduced into the WT BK channel cDNA in pcDNA3.1+ (GenBank MG279689; Supplemental Table 1). HEK-293T cells (CRL-11268, ATCC, Manassas, VA, USA) were maintained in DMEM media (Cat. #11995-065, Gibco, Life Technologies Corp., Grand Island, NY, USA) supplemented with 10% fetal bovine serum (Cat. #100-106, GeminiBio, West Sacramento, California, USA), 1% penicillin/streptomycin (Cat. #400-109, GeminiBio, West Sacramento, California, USA) and 1% L-glutamine (Cat. #25-005-Cl, Mediatech Inc., Manassas, VA, USA) in a humidified incubator at 37°C with 5% CO_2. Cells were transfected at 60–70% confluency with BK^{WT}, BK^{D434G}, BK^{N999S}, BK^{H444Q} or BK^{D965V} (see Supplemental Table 1 for residue numbering), and human $Ca_V1.2\alpha$ (*Cacna1c*, CAA84341.1), rat $Ca_V\beta1b$ (*Cacnb1*, CAA43665.1) and rat $Ca_V\alpha2\delta1$ (*Cacna2d1*, AAG28164.1) using Fugene HD (Fugent LLC Middleton, Wisconsin, USA) at 0.8:1:1:1 ratio of cDNA and a 1:6 ratio of transfection reagent (μg/μL). BK channel, $Ca_V1.2\alpha$, and $Ca_V\alpha2\delta1/\beta1b$ plasmids were prepared from 2–3, 5, and 2 independent plasmid preparations, respectively, and the numbers of independent transfections per condition were as follows: in EGTA (BK^{WT}, $n = 8$; BK^{D434G}, 9; BK^{N999S}, 8; BK^{H444Q}, 6; and BK^{D965V}, 4) and in BAPTA (BK^{WT}, $n = 9$; BK^{D434G}, 8; BK^{N999S}, 8; BK^{H444Q}, 4; and BK^{D965V}, 6). BK^{WT} was recorded alongside each mutation within the same week of data collection. After 24 hours, cells were washed with complete media containing Ca^{2+}-free minimum essential medium (Cat. #11380-037, Gibco, Life Technologies Corp., Grand Island, NY, USA) in place of DMEM. After 24–48 hours, cells were replated onto pre-treated glass coverslips with poly-L-lysine (Cat. #P4832, Sigma-Aldrich, St. Louis, MO, USA). Experimental recordings were performed 48–72 hours post-transfection.

Electrophysiological recordings

Macroscopic BK and Ca^{2+} currents were recorded in whole-cell voltage-clamp mode at 22–25°C with a MultiClamp 700B amplifier using electrodes (3–6 MΩ) filled with intracellular solution (123 mM K-methanesulfonate, 9 mM NaCl, 10 mM EGTA, 9 mM HEPES, 2 mM Mg-ATP and 2 mM Na_2-ATP, pH 7.3 (300–310 mOsm/kg)). BAPTA (5 mM) was substituted for EGTA in some internal solutions as specified in figure legends. The bath solution was composed of (125 mM NaCl, 1.2 mM $MgCl_2$, 1.25 mM NaH_2PO_4, 3.5 mM KCl, 2.5 mM $CaCl_2$, 10 mM HEPES and 10 mM D-glucose, pH 7.4 (~300 mOsm/kg)). The access resistance was <15 MΩ, and seal resistance was compensated 60–80%. Cells where R_s error > 20% were not included.

BK K^+ and $Ca_V1.2$ Ca^{2+}currents were isolated from total cell currents by bath application of 100 nM paxilline (Pax, Alomone Labs, Jerusalem, Israel, #P-450) as described in Figure 1b-d Pax was dissolved in DMSO (1000X) and focally applied to the bath at the concentrations listed above. Macroscopic currents were elicited from a holding potential of −90 mV in a two-part voltage protocol stepping for 50 ms from −100 to +60 mV in 20-mV increments followed by a second step to +60 mV for 50 ms. Ca^{2+} currents were assessed from the peak of the Ca^{2+} current from the first step, and K^+ currents were evaluated from the peak current from the second step of the subtracted BK channel current. Action potential-evoked currents were elicited from a holding potential of −90 mV following by an action potential voltage command derived from a previously recorded granule neuron waveform (baseline membrane potential, −47 mV; half-width, 1.9 ms; peak, +46 mV; AHP, −52 mV) [4].

Currents were sampled at 50 kHz and filtered online at 10 kHz with a P/5 leak subtraction protocol. Representative traces were post-hoc filtered at 2 kHz. Voltage values were adjusted for the liquid junction potential (10 mV). The Ca^{2+} current levels were obtained from the peak inward current elicited from the first voltage step after paxilline application, and the BK current was obtained from the peak outward current elicited from the second voltage step of the subtracted current. Currents were normalized to cell capacitance, and current density-voltage plots were constructed by plotting the current densities for each as a function of the voltage of the first step of the protocol, which elicits Ca^{2+} influx.

Statistics

All data were tested for normality with the Shapiro-Wilk test and either parametric or non-parametric statistical tests were performed. For parametric tests, one-way ANOVA with Bonferroni's post-hoc test was performed. For non-parametric tests, the Kruskal-Wallis testand Dunn's multiple comparisons test were performed. Statistical significance was determined at $p < 0.05$ using Prism v10, and significant p values are presented in the figure legends. Data are reported as group mean ± SEM.

Results

The goal of this study was to assess the BK current produced by channels containing one of four *KCNMA1* channelopathy associated mutations under dynamic activation by Ca^{2+} entry through voltage-gated $Ca_V1.2$ channels. Wild type (BK^{WT}) or mutant (BK^{D434G}, BK^{N999S}, BK^{H444Q} or BK^{D965V}) channels were co-expressed with $Ca_V1.2$ channels in HEK-293T cells. The auxiliary subunits $Ca_V\beta1b$ and $Ca_V\alpha2\delta1$ were expressed along with the $Ca_V\alpha1$ subunit due to their copurification from rat brain with both $Ca_V\alpha1$ and BKα, role in enhancing expression levels, requirement for normal gating properties, and high prevalence in neurons [24,32,44,45].

Macroscopic $Ca_V1.2$ and BK channel currents were recorded in the whole-cell voltage-clamp configuration, using a physiological K^+ gradient and 2.5 mM $[Ca^{2+}]_{ext}$. We employed a two-part voltage step protocol to activate the currents (Figure 1b). The first part comprised depolarizing voltage steps (−100 mV to +60 mV, Δ20 mV, 50 ms) to activate $Ca_V1.2$ channels and initiate Ca^{2+} influx (conditioning step). The second part was a test step to +60 mV (50 ms) to activate BK channels at a voltage that does not result in significant inward Ca^{2+} current ($E_{Ca2+} = +130$ mV, assuming a maximum $[Ca^{2+}]_i$ of 100 nM). Using this protocol, total whole-cell currents consisting of inward Ca^{2+} current through $Ca_V1.2$ channels, followed by outward K^+ current through BK channels, were elicited (Figure 1c). BK currents were pharmacologically isolated from $Ca_V1.2$ Ca^{2+} currents by application of 100 nM paxilline, a membrane permeant BK channel inhibitor (Figure 1d–e). These results show the sequential activation of $Ca_V1.2$ Ca^{2+} currents, followed by BK currents.

BK-Ca_V.2 channel currents under microdomain conditions

To assess the activation of wild type and mutant BK-$Ca_V1.2$ channels within a microdomain, whole-cell macroscopic current recordings were made in 10 mM intracellular EGTA buffering conditions [16,23]. Current density-voltage plots (I-Vs) were constructed from cells co-expressing

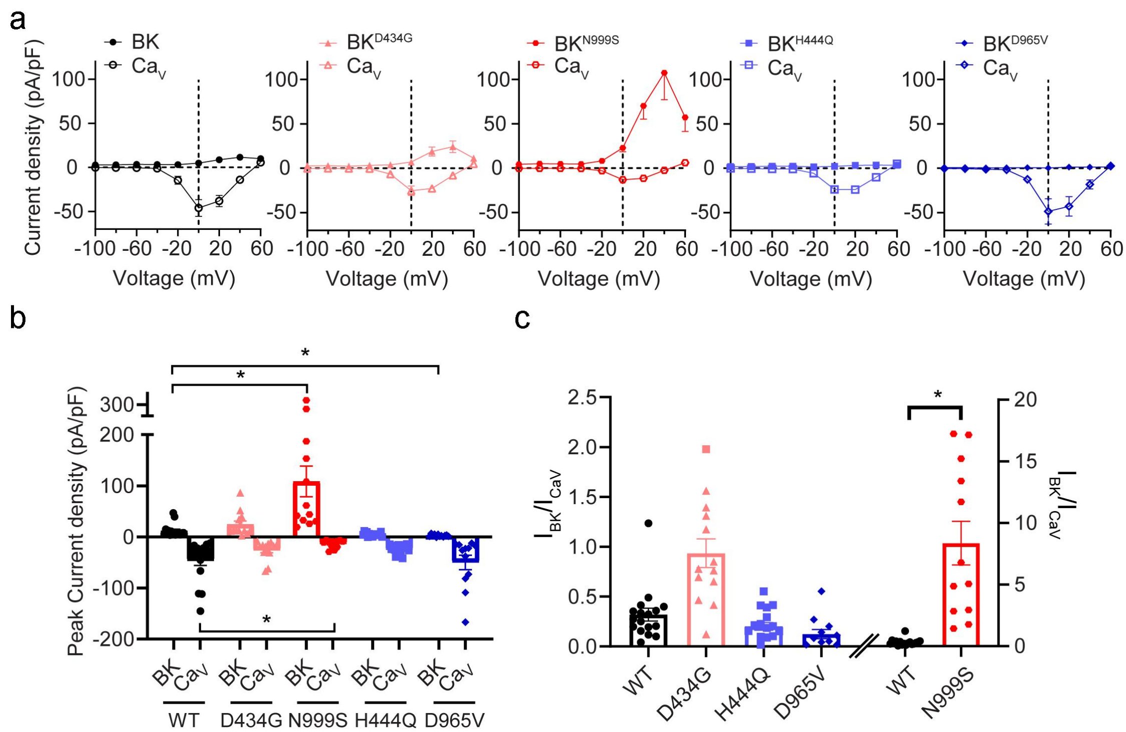

Figure 2. $Ca_V1.2$ and BK channel currents from cells co-expressing BK^{WT}, BK^{D434G}, BK^{N999S}, BK^{H444Q} and BK^{D965V} in 10 mM EGTA. (a) Current versus conditioning step voltage relationships for $Ca_V1.2$ and BK^{WT} (N = 17), BK^{D434G} (N = 13), BK^{N999S} (N = 12), BK^{H444Q} (N = 17) and BK^{D965V} (N = 12) channel currents plotted as a function of the first voltage step of the protocol which elicits Ca^{2+} influx. Representative traces are displayed in Supplemental Figure 1. (b) Peak $Ca_V1.2$ and BK channel current levels from (a). BK^{N999S} currents were larger ($p = 0.0034$), and BK^{D965V} currents were smaller ($p = 0.0122$), than BK^{WT}. Expanded y-axis view of BK current levels shown in Supplemental Figure 3. $Ca_V1.2$ (BK^{N999S}) currents were reduced compared to $Ca_V1.2$ (BK^{WT}; $p = 0.0003$). (c) Normalized current ratios (I_{BK}/I_{CaV}) were increased for $Ca_V1.2$ (BK^{D434G}; $p = 0.0572$) and $Ca_V1.2$ (BK^{N999S}; $p < 0.0001$) compared to $Ca_V1.2$ (BK^{WT}). BK^{WT} data on the right-hand side of the split x-axis is replotted for ease of comparison to BK^{N999S}. in B-C panels, values are plotted as individual measurements with average and s.e.m. p values < 0.05 were considered significant.

BK^{WT} channels with $Ca_V1.2$ channels (Figure 2a). BK^{WT}-$Ca_V1.2$ channel currents showed the inward Ca^{2+} current peaked at 0 mV. The outward K^+ current, from the second step in the voltage protocol to +60 mV, activated at depolarized voltages and peaked at +40 mV (Figure 2a, left panel). Ca^{2+} currents were assessed from the peak current density of the inward current from the first step, and K^+ currents were evaluated from the peak outward current density of the subtracted BK channel current from the second step (Figure 2b).

Next, we tested BK^{D434G}, BK^{N999S}, BK^{H444Q}, and BK^{D965V} mutant channels to determine if their activity under $Ca_V1.2$ activation was consistent with prior GOF and LOF designations derived from clamped $[Ca^{2+}]_i$ recordings [4,12,36,37,40]. Since both GOF channels exhibit faster activation compared to wild type, BK^{D434G} and BK^{N999S} channels were predicted to display increased BK current under $Ca_V1.2$ channel-mediated activation compared to BK^{WT}. Moreover, given the larger G-V shift and faster activation kinetics compared to BK^{D434G}, BK^{N999S} was predicted to have a greater impact on BK-Ca_V elicited K^+ current. Conversely, LOF channels activate slower than the wild type, and the delayed activation is anticipated to decrease BK^{H444Q} and BK^{D965V} channel currents under these conditions.

Ca^{2+} currents peaked around 0 mV (Figure 2a) and the levels were not significantly different between $Ca_V1.2$ channels co-expressed with BK^{WT} (−46 ± 9 pA/pF) and $Ca_V1.2$ co-expressed with BK^{D434G}, BK^{H444Q} or BK^{D965V} (−29 ± 5 pA/pF, −25 ± 2 pA/pF and −50 ± 14 pA/pF, respectively; Figure 2b). However, Ca^{2+} current from $Ca_V1.2$ (BK^{N999S}) was significantly decreased compared to the wild type, averaging −17 ± 3 pA/pF. As BK^{N999S} is the most severe GOF mutation [37], the observed difference between $Ca_V1.2$ (BK^{N999S}) and $Ca_V1.2$ (BK^{WT}) current densities may stem from limitations in clamping the particularly large currents induced by BK^{N999S} upon Ca^{2+} influx, causing more seals to break in this condition compared to others. It is possible that successful recordings were easier to obtain from cells with smaller $Ca_V1.2$ currents. It is also possible that these differences reflect differences in $Ca_V1.2$ expression levels, although this difference was not observed consistently for $Ca_V1.2$ (BK^{N999S}) across study conditions.

$Ca_V1.2$-activated BK channel currents peaked at +40 mV (Figure 2a–b). BK^{WT} current density averaged 12 ± 3 pA/pF. The current density of the GOF mutant BK^{N999S} was significantly larger than BK^{WT} at 109 ± 30 pA/pF, despite the lower Ca^{2+} current densities described above, while the current density of the LOF mutant BK^{D965V} was significantly smaller than BK^{WT} at 3 ± 1 pA/pF. However, the current densities of BK^{D434G} (25 ± 7 pA/pF) and BK^{H444Q} (5 ± 1 pA/pF) were not significantly different from BK^{WT}, and these respective measurements are plotted on an expanded scale in Supplemental Figure S3. Thus, the more severe GOF N999S and LOF D965V mutations both led to detectable differences in BK channel current density and in the expected directions, under $Ca_V1.2$ activation. Because these differences are similar to what has been observed for BK^{N999S} and BK^{D965V} under clamped calcium [1], it is likely that these differences arise from altered channel activity of these mutants.

In order to assess the current through wild type and mutant BK channels as a function of the available Ca^{2+} influx, the BK channel current was normalized to the absolute value of the peak inward $Ca_V1.2$ Ca^{2+} current shown in Figure 2b. In this analysis, GOF mutations should be more sensitive to Ca^{2+} influx than the wild type, resulting in a higher normalized current ratio (I_{BK}/I_{Cav}), while LOF mutations should be less sensitive, resulting in a lower ratio. I_{BKWT}/I_{Cav} averaged 0.3 ± 0.01, while $I_{BKN999S}/I_{Cav}$ was ~28 times greater at 8.4 ± 1.8. This large increase was not solely due to the voltage-dependent activation of BK^{N999S} channels, as no significant BK current was detected when BK^{N999S} channels were expressed alone in HEK-293T cells and activated using the same voltage protocols (data not shown). BK^{D434G} also showed a trend toward an increase in the I_{BK}/I_{Cav} ratio (0.9 ± 0.1). The normalized I_{BK}/I_{Cav} was not significantly changed with either LOF mutation compared to BK^{WT}. The BK channel current was also normalized to the maximum value of $Ca_V1.2$ Ca^{2+} total charge, which demonstrated identical statistically significant results as normalization to the peak inward $Ca_V1.2$ current (data not shown).

These data demonstrate that the GOF variant (N999S) shows a clear increase in BK channel current under voltage-gated $Ca_V1.2$ Ca^{2+} influx within an EGTA-buffered microdomain. The D434G, H444Q, and D965V patient variants did not exhibit distinguishable GOF or LOF behavior under these conditions, in contrast to what has been previously observed in clamped $[Ca^{2+}]_i$ recordings [4,12,35–40,43]. This result suggests that the dynamic diffusion of Ca^{2+} from $Ca_V1.2$ to BK channels within an EGTA-delimited microdomain can influence the extent of mutant BK channel phenotypes.

BK-Ca_V.2 channel currents under nanodomain conditions

While EGTA permits Ca^{2+} diffusion across tens to hundreds of nanometers, BAPTA restricts Ca^{2+} diffusion to a significantly smaller nanodomain around $Ca_V1.2$. Channels within nanodomains are tightly functionally coupled, typically due to co-localization proximity or direct interactions within neurons [14]. We next asked if the changes in current from $Ca_V1.2$-activated mutant BK channels persisted within nanodomains by recording currents in 2 mM BAPTA using the same two pulse voltage protocol. Under BAPTA conditions, $Ca_V1.2$ Ca^{2+} currents peaked between 0–20 mV (Figure 3a) and were smaller than the inward currents recorded in EGTA. $Ca_V1.2$ (BK^{WT}) current density averaged −13 ± 3 pA/pF (Figure 3b). There was no significant difference in $Ca_V1.2$ Ca^{2+} currents when $Ca_V1.2$ was co-expressed with BK^{D434G}, BK^{N999S} or BK^{H444Q}. However, $Ca_V1.2$ currents were significantly increased (−32 ± 8 pA/pF) when co-expressed with BK^{D965V} compared to BK^{WT}.

$Ca_V1.2$-activated BK^{WT} current density averaged 10 ± 2 pA/pF (Figure 3A–B). BK^{N999S} current density was significantly larger than BK^{WT} at 29 ±

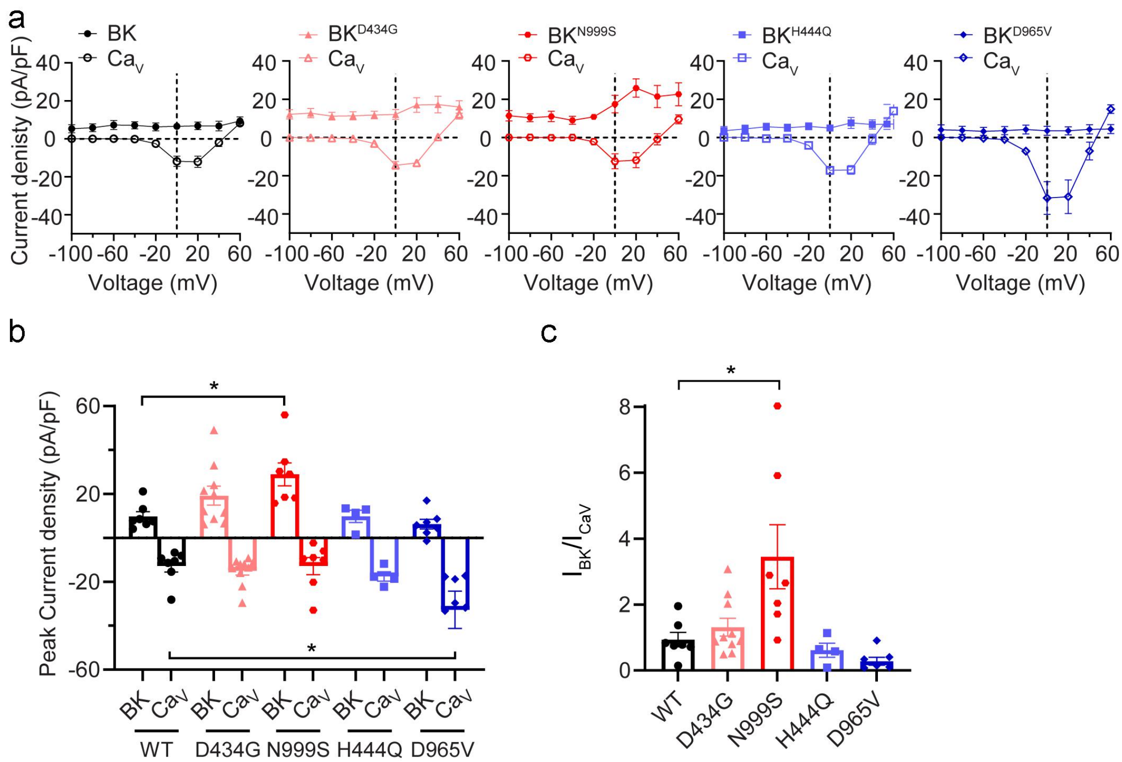

Figure 3. $Ca_V1.2$ and BK channel currents from cells co-expressing BK^{WT}, BK^{D434G}, BK^{N999S}, BK^{H444Q} and BK^{D965V} in 2 mM BAPTA. (A) Current versus conditioning step voltage relationships for $Ca_V1.2$ and BK^{WT} ($N = 7$), BK^{D434G} ($N = 10$), BK^{N999S} ($N = 7$), BK^{H444Q} ($N = 4$) and BK^{D965V} ($N = 7$) channel currents plotted as a function of the first voltage step of the protocol which elicits Ca^{2+} influx. Representative traces are displayed in Supplemental Figure 2. (B) Peak $Ca_V1.2$ and BK channel current levels from (A). BK^{N999S} currents were larger than BK^{WT} ($p = 0.0247$), and $Ca_V1.2$ (BK^{D965V}) currents were increased compared to $Ca_V1.2$ (BK^{WT})($p = 0.0099$). (C) Normalized current ratios (I_{BK}/I_{Cav}) were increased for $Ca_V1.2$ (BK^{N999S}; $p = 0.0319$) compared to $Ca_V1.2$ (BK^{WT}).

5 pA/pF, as it was in EGTA buffering conditions (Figure 2). Some of this BK^{N999S} current was detectable at hyperpolarized voltages in the absence of $Ca_V1.2$ expression (7.6 ± 1.2 pA/pF at −20 mV, $n = 5$), suggesting it results from the GOF effect of the N999S mutation. There were no statistically significant differences in BK current density between BK^{WT} and BK^{D434G}, BK^{H444Q}, or BK^{D965V} under 2 mM BAPTA buffering conditions. However, when BK channel current was normalized to the inward $Ca_V1.2$ Ca^{2+} current to assess BK channel current as a function of Ca^{2+} influx, the normalized I_{BKWT}/I_{Cav} averaged 0.8 ± 0.2 within BAPTA nanodomains (Figure 3c), higher than I_{BKWT}/I_{Cav} in EGTA (Figure 2c). Normalized $I_{BKN999S}/I_{Cav}$ current was ~4 times greater (3.5 ± 1) than I_{BKWT}/I_{Cav}. BK^{D434G}, BK^{H444Q} or BK^{D965V} showed no statistically significant difference in I_{BK}/I_{Cav} compared to BK^{WT}. Taken together, the data in Figures 2, 3 demonstrate that while the BK to $Ca_V1.2$ channel current ratio increases from a Ca^{2+} microdomain to a nanodomain, only the most severe GOF variant (N999S) produced an increase in both Ca^{2+} conditions. The GOF and LOF behaviors for the D434G, H444Q, or D965V variants shown in clamped $[Ca^{2+}]_i$ conditions were not recapitulated under activation by $Ca_V1.2$ Ca^{2+} current in heterologous cells.

BK-Ca_V.2 channel currents elicited by action potentials

We next applied single action potential voltage commands to test whether the observed effects of channelopathy mutations on BK channel current persist under conditions that use physiologically relevant stimuli to open $Ca_V1.2$ channels. During an action potential, changes in the voltage dependence of activation, as well as activation rate, will affect the peak BK current levels. Action potential-evoked currents were elicited from a holding potential of −90 mV, followed by an action potential voltage command obtained from a previously recorded dentate granule neuron waveform [4]. $Ca_V1.2$ and BK channel currents were recorded under microdomain and nanodomain buffering conditions.

In 10 mM EGTA, we found that $Ca_V1.2$ (BK^{WT}) current density averaged −35 ± 6 pA/pF, and there were no statistically significant differences between $Ca_V1.2$ (BK^{WT}) current density and that of $Ca_V1.2$ (BK^{D434G}), $Ca_V1.2$ (BK^{N999S}), $Ca_V1.2$ (BK^{H444Q}) and $Ca_V1.2$ (BK^{D965V}) under these conditions (Figure 4a). Outward BK^{WT} current density averaged 5 ± 2 pA/pF, and BK^{N999S} current density was significantly larger than BK^{WT} at 24 ± 7 pA/pF. BK^{D434G}, BK^{H444Q}, and BK^{D965V} currents were not statistically different from BK^{WT} (Figure 4b and Supplemental Figure S4). Normalized I_{BK}/I_{Cav} averaged 0.2 ± 0.02 for BK^{WT} (Figure 4c). $I_{BKN999S}/I_{Cav}$ was 1.3 ± 0.3, ~7 times greater than BK^{WT}; the other human patient variants showed no statistically significant difference in the I_{BK}/I_{Cav} ratio compared to BK^{WT}.

In 2 mM BAPTA (nanodomain) buffering conditions, $Ca_V1.2$ (BK^{WT}) current density averaged −50 ± 12 pA/pF (Figure 4d–e), and there were no statistically significant differences compared to $Ca_V1.2$ (BK^{D434G}), $Ca_V1.2$ (BK^{N999S}), $Ca_V1.2$ (BK^{H444Q}) or $Ca_V1.2$ (BK^{D965V}). Outward BK^{WT} current density averaged 25 ± 8 pA/pF, and BK^{N999S}, BK^{D434G}, and BK^{D965V} currents were not statistically different. Thus with BAPTA buffering, the increase in $Ca_V1.2$-activated BK^{N999S} current we observed under the two-step voltage protocol was not detectable under an action potential waveform voltage command. BK^{H444Q} showed a decrease in current density compared to BK^{WT} (10 ± 3 pA/pF). This was the only condition where the H444Q variant showed a significant effect on current. However, once the current density was normalized to assess I_{BK} as a function of I_{Cav}, no difference was observed between any of the

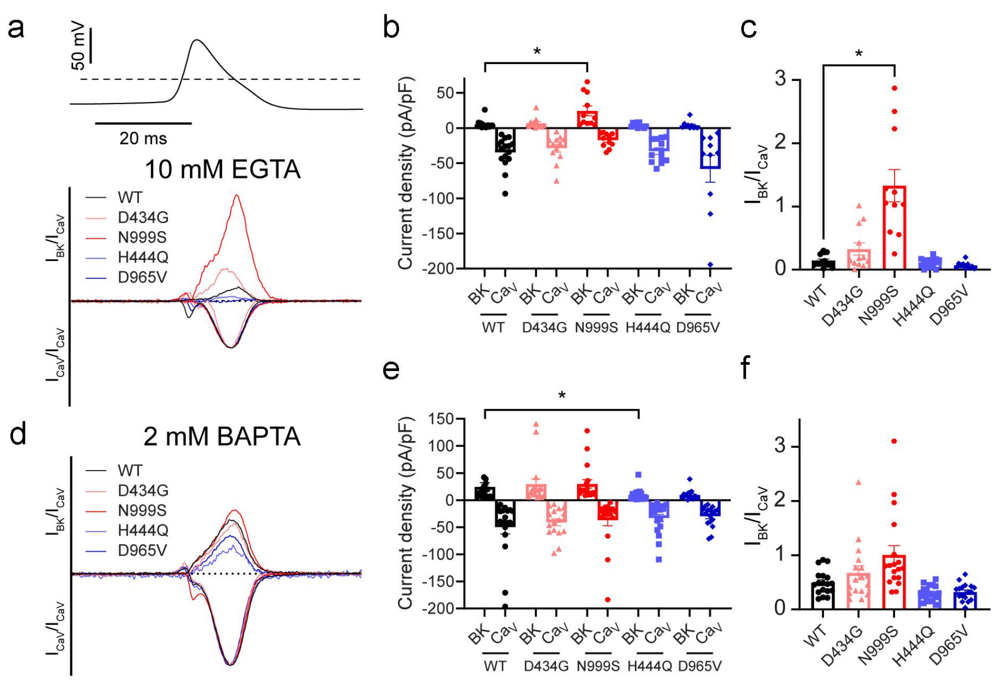

Figure 4. Action potential evoked $Ca_V1.2$ and BK channel currents from cells co-expressing BK^{WT}, BK^{D434G}, BK^{N999S}, BK^{H444Q} and BK^{D965V}. (A, D) Representative whole-cell $Ca_V1.2$ (inward) and BK (outward) currents from cells co-expressing $Ca_V1.2$ (BK^{WT}), $Ca_V1.2$ (BK^{D434G}), $Ca_V1.2$ (BK^{N999S}), $Ca_V1.2$ (BK^{H444Q}), and $Ca_V1.2$ (BK^{D965V}) channels in 10 mM EGTA (A) and 2 mM BAPTA (D). Traces are normalized to the absolute value of the peak $Ca_V1.2$ channel current. Dotted line represents zero current level. Insets: action potential voltage command. (B, E) BK and $Ca_V1.2$ channel currents from the peak of the action potential in 10 mM EGTA (B; $N = 10$-16 per condition) and 2 mM BAPTA (E; $N = 17$-18 per condition). BK^{N999S} current was larger than BK^{WT} in EGTA ($p = 0.0033$). BK^{H444Q} current was smaller than BK^{WT} in BAPTA ($p = 0.0422$). Expanded y-axis view of BK current levels in panel B shown in supplemental Figure 4. No significant differences in $Ca_V1.2$ currents were observed. (C, F) normalized current ratios (I_{BK}/I_{Cav}) in 10 mM EGTA (C) and 2 mM BAPTA (F). $Ca_V1.2$ (BK^{N999S}) channel current was larger compared to $Ca_V1.2$ (BK^{WT}) in EGTA ($p = 0.003$) but not statistically significant in BAPTA ($p = 0.0643$).

variants (Figure 4f). This result indicates that under certain conditions, such as the rapid BAPTA buffering and millisecond depolarization from a single action potential, even the strong GOF mutant BK^{N999S} channels are unable to produce a detectable difference in $Ca_V1.2$-activated BK current.

Discussion

This study describes the relative BK current levels associated with four representative *KCNMA1* channelopathy variants compared to the wild type under $Ca_V1.2$ activation. N999S is the most common patient variant and causes more severe neurological disease than the other variants tested in this study [1,4]. In clamped Ca^{2+} recordings, N999S produces strong GOF changes in multiple aspects of BK channel gating [36,37]. Consistent with this, $Ca_V1.2$-activated BK^{N999S} current showed increased steady-state current within both microdomain (EGTA) and nanodomain (BAPTA) Ca^{2+} buffering conditions (Figures 2,3). Importantly, an increase in $Ca_V1.2$-activated BK^{N999S} current was also evident when the BK current was analyzed as a function of the $Ca_V1.2$ current magnitude, suggesting that these results reflect the underlying GOF properties of the BK^{N999S} channels and are not due to changes in the Ca^{2+} current.

While steady-state currents recorded under clamped Ca^{2+} allow maximal activation of BK channels, we found that the BK^{N999S} GOF effect was still detectable when $Ca_V1.2$-activated BK channel current was evoked using an action potential command within Ca^{2+} microdomain conditions. The activation for $Ca_V1.2$ channels ranges from 1–5 ms, depending on membrane potential and auxiliary subunit composition [28,46], and $Ca_V1.2$ channels do not achieve maximal P_o during short single spikes [28]. The time to peak for the neuronal action potential voltage command used in this study was <0.5 ms [4], and the nanodomain context would further reduce Ca^{2+}-dependent activation. Under this condition, the BK^{N999S} GOF effect, suggesting that the Ca^{2+} channel openings and BK-Ca_V coupling context is an important determinant of the GOF current produced by mutant BK^{N999S} channels.

In contrast, the other channelopathy mutations did not show the systematic set of changes across conditions in $Ca_V1.2$-activated mutant BK channel current that were observed for N999S. This finding parallels the results from mouse models generated from these mutations. Interestingly, the GOF D434G variant causes similar neurological phenotypes as N999S, but in smaller subset of human patients [38] and with a comparatively milder phenotype in transgenic mice [4]. The LOF H444Q variant is found in a single individual and does not recapitulate the full channelopathy disease phenotype in mice [4]. The D965V variant has also only been found in a single individual so far and has not been tested yet in a transgenic animal model. Thus, finding alterations in $Ca_V1.2$-activated BK current for only one of the mutations tested in this study was different from previous work performed in clamped Ca^{2+} conditions, where all four mutations showed significant differences from the wild type [1]. These results suggest that 1) testing *KCNMA1* variants in BK channels recorded in clamped Ca^{2+} conditions using steady-state voltage protocols may overestimate the potential for pathogenicity, and 2) cellular buffering and dynamic voltage stimuli may differentially affect Ca_V channel activation of mutant BK channel currents. It remains to be determined whether these contextual elements explain some of the heterogeneity observed in *KCNMA1* channelopathy.

Several factors may account for the differences between BK channel activation under steady-state and Ca_V channel mediated Ca^{2+} influx, including the type of biophysical alteration produced by the respective channelopathy mutations, the use of paxilline to isolate the BK current, the respective expression levels of BK and $Ca_V1.2$ channels, the strength of coupling between BK and Ca_V channels, and any feedback of BK current on Ca^{2+} influx. With respect to the biophysical basis of BK channel mutations, the two mutations identified as GOF in clamped Ca^{2+} conditions differ mechanistically. N999S acts by enhancing voltage sensitivity, and BK^{N999S} channels exhibit a 1.5-fold larger G-V shift and ~3.5-fold faster activation time constant than BK^{D434G} channels [37]. Eliminating calcium-dependent activation in BK^{N999S} channels does not affect the G-V shift [36]. This predominant voltage mechanism could support the GOF activity of BK^{N999S} channels under a wider range of Ca^{2+} conditions than BK^{D434G} channels. Conversely, BK^{D434G} channels demonstrate increased Ca^{2+} sensitivity in clamped Ca^{2+} recording conditions [38–40,42], a finding that could connect their activation more closely to the Ca^{2+} buffering or BK-Ca_V coupling context. BK^{D434G} channels also exhibit a more pronounced hyperpolarizing $V_{1/2}$ shift in the mid-range of $[Ca^{2+}]_i$, suggesting that this GOF mutation may behave nonlinearly under dynamic $Ca_V1.2$ activation. A single study has probed the activation of BK^{D434G} channels by a Ca_V channel ($Ca_V2.2$; N-type). Under those study conditions, $Ca_V2.2$-activated BK^{D434G} channel current showed an acceleration of BK channel activation and reduction in activation lag time compared to BK^{WT} [31]. For LOF mutations characterized in clamped Ca^{2+} conditions, the biophysical basis for changes in BK^{H444Q} and BK^{D965V} channel gating has not been reported. Both mutations localize to regions of the BK channel gating ring that are involved in Ca^{2+}-dependent activation. The effect of each of these LOF mutations is smaller than the absolute effect of either N999S or D434G [1,4,12], consistent with the data in this study.

Use of paxilline to isolate the BK current also has a possibility of differentially affecting currents from GOF versus LOF mutations, based on the inverse relationship of paxilline and BK channel open probability. Paxilline inhibition was lower with closed channels compared to maximally open channels, and this relationship is also Ca^{2+} modulated [47]. Although the patient mutations tested here are not expected to affect paxilline binding based on their locations [48], it is also possible that paxilline affinity differs between mutations. These possibilities await further testing in experiments that specifically control BK channel open probability for each mutation. Such experiments may also be informative for understanding the therapeutic potential of paxilline and related compounds for myotonia [49].

Another factor influencing the functional designations derived from clamped Ca^{2+} and Ca_V-mediated BK channel activation conditions is the relative expression level of each channel type, which was not assessed in this study. Differing BK-Ca_V expression ratios would not be relevant for activating BK channels in clamped Ca^{2+} but could affect the stoichiometry and coupling strength of $Ca_V1.2$-BK channel complexes. The assessment of BK-Ca_V channel currents in the two buffering conditions tested in this study (EGTA and BAPTA) likely reflects different coupling scenarios, with the EGTA condition including less tightly coupled channels than the BAPTA condition. This is supported by the decrease in Ca_V-activated BK channel current observed between EGTA and BAPTA. However, the stoichiometry of these coupled channels cannot be assessed in this study and is not resolved in other studies. Some models have suggested a fixed Ca_V to BK channel stoichoimetry (Prakriya & Lingle, 2000) [20,23], while other investigations only demonstrated a statistical bias for Ca_V and BK channel proximity with no fixed stoichiometry or geometry within the clusters (Vivas et al., 2017). Additionally, scaffolding proteins could regulate the spatial arrangement of BK-Ca_V complexes [50], yet it is not known if these proteins function similarly in native and heterologous systems. Interestingly, higher BK channel expression has been shown to compete α2δ away from $Ca_V2.2$ channels, reducing the Ca^{2+} current density [17]. Thus, how the summation of expression affects coupling of BK-Ca_V channels remains to be determined.

There are two conditions where $Ca_V1.2$ currents are altered by co-expression with mutant BK channels in this study: BK^{N999S} (EGTA) and BK^{D965V} (BAPTA). It is possible that recordings for these two variants were easier to obtain from cells that had smaller Ca^{2+} currents for the GOF mutation and larger Ca^{2+} currents for the LOF mutation. However, since the Ca^{2+} current changes were not observed consistently across conditions, whether there is a relevant underlying biological mechanism related to the BK channel mutations or variation in expression related to the mutations remains to be determined. Such a mechanism could involve functional feedback of the BK current on activation of the Ca^{2+} channel or an altered interaction between those particular mutants and $Ca_V1.2$ subunits. Expression, stoichiometry, and coupling are difficult to control in heterologous expression systems using high copy plasmids, and future studies specifically designed to address whether the mutations cause differences in expression and assembly of BK-$Ca_V1.2$ complexes will be needed. In addition, patients harbor heterozygous alleles, creating the potential for heterotetrameric BK channels [51]. Nevertheless, this study was able to evaluate the effects of these BK channel mutations by normalizing BK current to the Ca^{2+} current.

While the central finding of this work was the corroboration of the GOF effect of N999S variant under $Ca_V1.2$-mediated BK channel activation, the results for the three other representative channelopathy variants illustrate that the effects of *KCNMA1* variants could be highly neuron dependent. Important contextual variations could include different Ca_V subunits, Ca^{2+} buffering conditions known to affect coupling strength and type of gating stimuli (waveform and frequency of action potentials). Examining the effects of BK channelopathy mutations in a wider range of contexts, such as within different neuronal types, may yield more realistic predictions about the pathogenicity of novel variants. Improved predictions will provide a more detailed understanding of how dysregulation of BK channel gating may lead to altered neuronal excitability and support stronger genotype-phenotype correlations in *KCNMA1*-linked disease.

Acknowledgments

We thank Ivy Dick and Joerg Striessnig for the Ca^{2+} channel cDNA constructs and Hans Moldenhauer for data discussions. Figure 1a created with Biorender.com.

Disclosure statement

No potential conflict of interest was reported by the author(s).

Funding

This work was funded by NHLBI R01-HL102758 (ALM) and the NIGMS ASCEND Scholars Program Grant 2RL5GM118972. National Institute of General Medical Sciences [ASCEND Scholars Program Grant 2RL5GM118972]; National Heart Lung and Blood Institute [R01HL102758]

Author contributions

R.L. Dinsdale: research conception and data collection, data analysis, statistical analysis design and execution, and manuscript writing. A.L. Meredith: research conception, data analysis, and manuscript writing. All authors approved the final version of the manuscript.

Data availability statement

The data are available from the corresponding author, ALM, upon reasonable request.

ORCID

Ria L. Dinsdale http://orcid.org/0000-0003-1384-5582
Andrea L. Meredith http://orcid.org/0000-0003-1061-2302

References

[1] Meredith AL. BK channelopathies and *KCNMA1*-linked disease models. Annu Rev Physiol. 2024 [Feb 12];86(1):277–300. doi: 10.1146/annurev-physiol-030323-042845
[2] Bailey CS, Moldenhauer HJ, Park SM, et al. *KCNMA1*-linked channelopathy. J Gen Physiol. 2019 [Oct 7];151 (10):1173–1189. doi: 10.1085/jgp.201912457
[3] Miller JP, Moldenhauer HJ, Keros S, et al. An emerging spectrum of variants and clinical features in *KCNMA1*-linked channelopathy. Channels (Austin). 2021 [Dec;15 (1):447–464. doi: 10.1080/19336950.2021.1938852
[4] Park SM, Roache CE, Iffland PH. 2nd, BK channel properties correlate with neurobehavioral severity in three *KCNMA1*-linked channelopathy mouse models. Elife. 2022 [Jul 12];11:e77953. doi: 10.7554/eLife.77953 et al.
[5] Dong P, Zhang Y, Hunanyan AS, et al. Neuronal mechanism of a BK channelopathy in absence epilepsy and dyskinesia. Proc Natl Acad Sci. 2022 [Mar 22];119 (12):e2200140119. doi: 10.1073/pnas.2200140119
[6] Dinsdale RL, Roache CE, Meredith AL. Disease-associated *KCNMA1* variants decrease circadian clock robustness in channelopathy mouse models. J Gener Physiol. 2023;155(11). doi: 10.1085/jgp.202313357
[7] Sun AX, Yuan Q, Fukuda M, et al. Potassium channel dysfunction in human neuronal models of Angelman syndrome. Science. 2019 [Dec 20];366(6472):1486–1492. doi: 10.1126/science.aav5386
[8] Zhu Y, Zhang S, Feng Y, et al. The Yin and Yang of BK channels in epilepsy. CNS Neurol Disord Drug Targets. 2018;17(4):272–279. doi: 10.2174/1871527317666180213142403

[9] Perche O, Lesne F, Patat A, et al. Large-conductance calcium-activated potassium channel haploinsufficiency leads to sensory deficits in the visual system: a case report. J Med Case Rep. 2022 [May 5];16(1):180. doi: 10.1186/s13256-022-03387-7

[10] Du X, Carvalho-de-Souza JL, Wei C, et al. Loss-of-function BK channel mutation causes impaired mitochondria and progressive cerebellar ataxia. Proc Natl Acad Sci USA. 2020 [Mar 4];117(11):6023–6034. doi: 10.1073/pnas.1920008117

[11] Deng PY, Klyachko VA. Genetic upregulation of BK channel activity normalizes multiple synaptic and circuit defects in a mouse model of fragile X syndrome. J Physiol. 2016 [Jan 1];594(1):83–97. doi: 10.1113/JP271031

[12] Moldenhauer HJ, Tammen K, Meredith AL. Structural mapping of patient-associated *KCNMA1* gene variants. Biophys J. 2024 [Jul 16];123(14):1984–2000. doi: 10.1016/j.bpj.2023.11.3404

[13] Tao X, MacKinnon R. Molecular structures of the human Slo1 K^+ channel in complex with beta4. Elife. 2019 [Dec 9];8. doi: 10.7554/eLife.51409

[14] Shah KR, Guan X, Yan J. Structural and functional coupling of calcium-activated BK channels and calcium-permeable channels within nanodomain signaling complexes. Front Physiol. 2022;12:12. doi: 10.3389/fphys.2021.796540

[15] Raimondo JV, Burman RJ, Katz AA, et al. Ion dynamics during seizures [review]. Front Cell Neurosci. 2015 [Oct 21];9. doi: 10.3389/fncel.2015.00419

[16] Fakler B, Adelman JP. Control of K_{Ca} channels by calcium nano/microdomains [review]. Neuron. [2008 Sep 25];59(6):873–881. doi: 10.1016/j.neuron.2008.09.001

[17] Zhang FX, Gadotti VM, Souza IA, et al. BK potassium channels suppress Cavalpha2delta subunit function to reduce inflammatory and neuropathic pain. Cell Rep. 2018 [Feb 20];22(8):1956–1964. doi: 10.1016/j.celrep.2018.01.073

[18] Rehak R, Bartoletti TM, Engbers JD, et al. Low voltage activation of KCa1.1 current by Cav3-KCa1.1 complexes. PLoS One. 2013;8(4):e61844. doi: 10.1371/journal.pone.0061844

[19] Augustine GJ, Santamaria F, Tanaka K. Local calcium signaling in neurons. Neuron. 2003 [Oct 9];40(2):331–346. doi: 10.1016/S0896-6273(03)00639-1

[20] Fakler B, Adelman JP. Control of K(Ca) channels by calcium nano/microdomains. Neuron. 2008 [Sep 25];59(6):873–881. doi: 10.1016/j.neuron.2008.09.001

[21] Naraghi M, Neher E. Linearized buffered Ca^{2+} diffusion in microdomains and its implications for calculation of $[Ca^{2+}]$ at the mouth of a calcium channel. J Neurosci. 1997 [Sep 15];17(18):6961–6973. doi: 10.1523/JNEUROSCI.17-18-06961.1997

[22] Vivas O, Moreno CM, Santana LF, et al. Proximal clustering between BK and $Ca_V1.3$ channels promotes functional coupling and BK channel activation at low voltage. Elife. 2017 [Jun 30]:e28029 doi: 10.7554/eLife.28029

[23] Cox DH. Modeling a Ca^{2+} channel/BK_{Ca} channel complex at the single-complex level. Biophys J. 2014 [Dec 16];107(12):2797–2814. doi: 10.1016/j.bpj.2014.10.069

[24] Berkefeld H, Sailer CA, Bildl W, et al. BK_{Ca}-Ca_V channel complexes mediate rapid and localized Ca^{2+}-activated K^+ signaling. Science. 2006 [Oct 27];314(5799):615–620. doi: 10.1126/science.1132915

[25] Engbers JD, Zamponi GW, Turner RW. Modeling interactions between voltage-gated Ca^{2+} channels and KCa1.1 channels. Channels (Austin). 2013 [Nov-Dec];7(6):524–529. doi: 10.4161/chan.25867

[26] Whitt JP, Ba M, Meredith AL. Differential contribution of Ca^{2+} sources to day and night BK current activation in the circadian clock. J Gen Physiol. 2018 [Feb 5];150(2):259–275. doi: 10.1085/jgp.201711945

[27] Plante AE, Whitt JP, Meredith AL. BK channel activation by L-type Ca^{2+} channels $Ca_V.2$ and $Ca_V.3$ during the subthreshold phase of an action potential. J Neurophysiol. 2021 [Aug 1];126(2):427–439. doi: 10.1152/jn.00089.2021

[28] Berkefeld H, Fakler B. Repolarizing responses of BK_{Ca}-Cav complexes are distinctly shaped by their cav subunits. J Neurosci. 2008 [Aug 13];28(33):8238–8245. doi: 10.1523/JNEUROSCI.2274-08.2008

[29] Blömer LA, Giacalone E, Abbas F, et al. Kinetics and functional consequences of BK channels activation by N-type Ca^{2+} channels in the dendrite of mouse neocortical layer-5 pyramidal neurons. Front Cell Neurosci. 2024 2024-Feb 14;18:18. doi: 10.3389/fncel.2024.1353895

[30] Loane DJ, Lima PA, Marrion NV. Co-assembly of N-type Ca^{2+} and BK channels underlies functional coupling in rat brain. J Cell Sci. 2007 [Mar 15];120(Pt 6):985–995. doi: 10.1242/jcs.03399

[31] Berkefeld H, Fakler B. Ligand-gating by Ca^{2+} is rate limiting for physiological operation of BK_{Ca} channels. J Neurosci. 2013 [Apr 24];33(17):7358–7367. doi: 10.1523/JNEUROSCI.5443-12.2013

[32] Catterall WA. Voltage-gated calcium channels. Cold Spring Harb Perspect Biol. 2011 Aug;3(8):a003947. doi: 10.1101/cshperspect.a003947

[33] Grunnet M, Kaufmann WA. Coassembly of big conductance Ca^{2+}-activated K^+ channels and L-type voltage-gated Ca^{2+} channels in rat brain. J Biol Chem. 2004 [Aug 27];279(35):36445–36453. doi: 10.1074/jbc.M402254200

[34] Herold KG, Hussey JW, Dick IE. *CACNA1C*-Related channelopathies. Handb Exp Pharmacol. 2023;279:159–181.

[35] Liang L, Liu H, Bartholdi D, et al. Identification and functional analysis of two new de novo *KCNMA1* variants associated with Liang–Wang syndrome. Acta Physiol. 2022 Feb;13(1):e13800. doi: 10.1111/apha.13800

[36] Li X, Poschmann S, Chen Q, et al. De Novo BK channel variant causes epilepsy by affecting voltage gating but not Ca^{2+} sensitivity. Eur J Hum Genet. 2018 Feb;26(2):220–229. doi: 10.1038/s41431-017-0073-3

[37] Moldenhauer HJ, Matychak KK, Meredith AL. Comparative gain-of-function effects of the *KCNMA1*-N999S mutation on human BK channel properties. J Neurophysiol. 2020 [Feb 1];123(2):560–570. doi: 10.1152/jn.00626.2019
[38] Du W, Bautista JF, Yang H, et al. Calcium-sensitive potassium channelopathy in human epilepsy and paroxysmal movement disorder. Nat Genet. 2005 Jul;37(7):733–738. doi: 10.1038/ng1585
[39] Wang B, Rothberg BS, Brenner R. Mechanism of increased BK channel activation from a channel mutation that causes epilepsy. J Gen Physiol. 2009 Mar;133(3):283–294. doi: 10.1085/jgp.200810141
[40] Yang J, Krishnamoorthy G, Saxena A, et al. An epilepsy/dyskinesia-associated mutation enhances BK channel activation by potentiating Ca^{2+} sensing. Neuron. 2010 [Jun 24];66(6):871–883. doi: 10.1016/j.neuron.2010.05.009
[41] Plante AE, Lai MH, Lu J, et al. Effects of single nucleotide polymorphisms in human *KCNMA1* on BK current properties. Front Mol Neurosci. 2019;12:285. doi: 10.3389/fnmol.2019.00285
[42] Diez-Sampedro A, Silverman WR, Bautista JF, et al. Mechanism of increased open probability by a mutation of the BK channel. J Neurophysiol. 2006 Sep;96(3):1507–1516. doi: 10.1152/jn.00461.2006
[43] Moldenhauer H, Park SM, Meredith AL. Characterization of new human *KCNMA1* loss-of-function mutations. Biophys J. 2020;118(3):114a. doi: 10.1016/j.bpj.2019.11.767
[44] Dolphin AC. The alpha2delta subunits of voltage-gated calcium channels. Biochim Biophys Acta. 2013 Jul;1828(7):1541–1549. doi: 10.1016/j.bbamem.2012.11.019
[45] Ferrandiz-Huertas C, Gil-Minguez M, Lujan R. Regional expression and subcellular localization of the voltage-gated calcium channel beta subunits in the developing mouse brain. J Neurochem. 2012 Sep;122(6):1095–1107. doi: 10.1111/j.1471-4159.2012.07853.x
[46] Helton TD, Xu W, Lipscombe D. Neuronal L-type calcium channels open quickly and are inhibited slowly. J Neurosci. 2005 [Nov 2];25(44):10247–10251. doi: 10.1523/JNEUROSCI.1089-05.2005
[47] Zhou Y, Lingle CJ. Paxilline inhibits BK channels by an almost exclusively closed-channel block mechanism. J Gen Physiol. 2014 Nov;144(5):415–440. doi: 10.1085/jgp.201411259
[48] Zhou Y, Xia XM, Lingle CJ. The functionally relevant site for paxilline inhibition of BK channels. Proc Natl Acad Sci. 2020 [Jan 14];117(2):1021–1026. doi: 10.1073/pnas.1912623117
[49] Hoppe K, Sartorius T, Chaiklieng S, et al. Paxilline prevents the onset of myotonic stiffness in pharmacologically induced myotonia: a preclinical investigation. Front Physiol. 2020;11:533946. doi: 10.3389/fphys.2020.533946
[50] Sclip A, Acuna C, Luo F, et al. Rim-binding proteins recruit bk-channels to presynaptic release sites adjacent to voltage-gated Ca^{2+}-channels. Embo J. 2018 [Aug 15];37(16). doi: 10.15252/embj.201798637
[51] Geng Y, Li P, Butler A, et al. BK channels of five different subunit combinations underlie the de novo KCNMA1 G375R channelopathy. J Gen Physiol. 2023 [May 1];155(5):e202213302. doi: 10.1085/jgp.202213302